Journal of Computational Physics 439 (2021) 110393

Contents lists available at ScienceDirect

Journal of Computational Physics

www.elsevier.com/locate/jcp

A variable Eddington factor method with different spatial discretizations for the radiative transfer equation and the hydrodynamics/radiation-moment equations

Jijie Lou *, Jim E. Morel

Department of Nuclear Engineering, Texas A&M University, College Station, TX 77843, USA

ARTICLE INFO

Article history:
Available online 30 April 2021

Keywords:
Variable Eddington factor
Discontinuous Galerkin
Mixed finite-element
Radiation-hydrodynamics

ABSTRACT

The purpose of this paper is to present a High-Order/Low-Order radiation-hydrodynamics method that is second-order accurate in both space and time and uses the Variable Eddington Factor (VEF) method to couple a high-order set of 1-D slab-geometry grey S_n radiation transport equations with a low-order set of radiation moment and hydrodynamics equations. The S_n equations are spatially discretized with a lumped linear-discontinuous Galerkin scheme, while the low-order radiation-hydrodynamics equations are spatially discretized with a constant-linear mixed finite-element scheme. Both the high-order and low-order equations are discretized in time using a trapezoidal BDF-2 method. One manufactured solution is used to demonstrate that the scheme is second-order accurate for smooth solutions, and another one is used to demonstrate that the scheme is asymptotic-preserving in the equilibrium-diffusion limit. Calculations are performed for radiative shock problems and compared with semi-analytic solutions. In a previous paper it was shown that the pure radiative transfer scheme (the S_n equations coupled to the radiation moment equations and a material temperature equation rather than the hydrodynamics equations) is asymptotic-preserving in the equilibrium-diffusion limit, is well-behaved with unresolved spatial boundary layers in that limit, and yields accurate Marshak wave speeds even with strongly temperature-dependent opacities and relatively coarse meshes. These same properties carry over to our radiation-hydrodynamics scheme.

Published by Elsevier Inc.

1. Introduction

The purpose of this paper is to present a High-Order/Low-Order (HOLO) radiation-hydrodynamics method that is second-order accurate in both space and time and uses the Variable Eddington Factor (VEF) method to couple a high-order set of grey 1-D slab-geometry S_n radiation transport equations with a low-order set of radiation moment and hydrodynamics equations. The Variable Eddington Factor method, also known as the quasi-diffusion method, is a classic nonlinear method for accelerating source iterations in S_n transport calculations [1]. The S_n equations are spatially discretized with a lumped linear-discontinuous Galerkin scheme, while the low-order radiation-hydrodynamics equations are spatially discretized with a constant-linear mixed finite-element scheme. Both the high-order and low-order equations are discretized in time using

* Corresponding author.
E-mail addresses: loujijie1991@tamu.edu (J. Lou), morel@tamu.edu (J.E. Morel).

https://doi.org/10.1016/j.jcp.2021.110393
0021-9991/Published by Elsevier Inc.

a particular form of the trapezoidal BDF-2 method [2]. The motivation for this scheme arose from the BLAST radiation-hydrodynamics code [3] being developed at Lawrence Livermore National Laboratory. The hydrodynamics in BLAST is spatially-discretized using high-order mixed finite-element methods, but such discretizations are known to be inappropriate for the S_n equations. This work is intended to serve as a proof-of-principle that the VEF approach can be used to efficiently and accurately couple the high-order S_n equations spatially discretized with a standard lumped linear-discontinuous Galerkin method to a set of low-order radiation-hydrodynamics equations spatially discretized with the standard constant-linear mixed finite-element method. It was shown in Lou, Morel, and Gentile [4] that the pure radiative transfer version of our scheme (the S_n equations coupled to radiation moment equations and a material temperature equation rather than the hydrodynamics equations) is asymptotic-preserving in the equilibrium-diffusion limit, well-behaved in this limit with unresolved spatial boundary layers, and yields accurate Marshak wave speeds even with strongly temperature-dependent opacities and relatively coarse meshes. These same properties carry over to our radiation-hydrodynamics scheme.

The remainder of this paper is organized as follows. First we describe the equations of radiation-hydrodynamics that we solve. Next we discuss the radiation moment equations and variable Eddington factor. We then give a high-level overview of our HOLO VEF scheme, followed by the temporally-differenced equations in spatially continuous form. Our space-time discretization schemes for the S_n equations and low-order radiation-hydrodynamics equations are then briefly described. Computational results are presented next. We first demonstrate the second-order accuracy of our method in space and time for smooth problems. We next demonstrate that our method is asymptotic-preserving in the equilibrium-diffusion limit. We conclude this section with a comparison of results for radiative shock solutions using our method with semi-analytic benchmark solutions. Finally, we give conclusions and suggestions for future work.

2. The equations of radiation-hydrodynamics

In this section we describe the equations we solve, which consist of the grey radiative transfer equation coupled to the non-relativistic Lagrangian hydrodynamics equations in 1-D Cartesian geometry. We express time in shakes (sh) and photon energy in jerks (jk). One shake is 10^{-8} seconds, and one jerk is 10^9 joules. These units are traditionally used in the high-energy density laboratory physics community and supposedly were originally defined to make the radiation constant of order 1 due to the severely restricted range of numerical values allowed by early computers.

The radiation transport equation is given by:

$$\frac{\rho}{c}\frac{D}{Dt}\left(\frac{\psi}{\rho}\right)+\frac{\partial}{\partial x}\left[\left(\mu-\frac{u}{c}\right)\psi\right]+\sigma_t\psi=\frac{\sigma_s}{4\pi}\phi+\frac{\sigma_a}{4\pi}acT^4-\frac{1}{4\pi}\frac{\sigma_t}{c}\mathcal{F}_0 u+\frac{\mu}{\pi}\frac{\sigma_t}{c}\phi u\,, \tag{1}$$

where

$$\phi=c\mathcal{E}\,, \tag{1a}$$

$$\mathcal{E}=\frac{1}{c}2\pi\int_{-1}^{+1}\psi\,d\mu\,, \tag{1b}$$

$$\mathcal{F}_0=\mathcal{F}-\frac{4}{3}\phi\frac{u}{c}\,, \tag{1c}$$

$$\mathcal{F}=2\pi\int_{-1}^{+1}\mu\psi\,d\mu\,, \tag{1d}$$

where the speed of light is denoted by $c\ cm/sh$, the radiation constant is denoted by $a\ jk/cm^3-keV^4$, the radiation angular intensity is denoted by ψ $(jk/cm^2-sh-steradian)$, the angle-integrated radiation intensity is denoted by ϕ (jk/cm^2-sh), the radiation energy density is denoted by $\mathcal{E}$ (jk/cm^3), the radiation flux is denoted by $\mathcal{F}$ (jk/cm^2-s), the comoving-frame radiation flux is denoted by $\mathcal{F}_0$ (jk/cm^2), the mass density is denoted by ρ (g/cm^3), the material velocity is denoted by u (cm/sh), the material temperature is denoted by T (keV), the macroscopic absorption cross section is denoted by σ_a (cm^{-1}) and the macroscopic scattering cross section is denoted by σ_s (cm^2/g). A macroscopic cross section, σ, can be expressed in terms of a corresponding opacity, κ (cm^2/g) as follows: $\sigma=\rho\kappa$. The Lagrangian hydrodynamics equations are given by the material momentum equation:

$$\rho\frac{Du}{D}t=-\frac{\partial p}{\partial x}+\frac{\sigma_t}{c}\mathcal{F}_0\,, \tag{2}$$

the internal energy equation:

$$\rho \frac{De}{D}t + p\frac{\partial u}{\partial x} = \sigma_a \left(\phi - acT^4\right), \tag{3}$$

and the equations of state:

$$p = \rho e(\gamma - 1), \tag{4}$$

$$\frac{\partial e}{\partial T} = C_v. \tag{5}$$

The material pressure is denoted by p (jk/cm^3), the specific material internal energy is denoted by e (jk/g), the specific heat is denoted by C_v $(jk/g - keV)$. The conservation of mass equation is generally not included in the Lagrangian hydrodynamics equations because it has an indeterminant Lagrangian form that cannot be used to solve for the mass density. Rather one simply uses the fact that mass within a volume moving with the fluid is constant. Because we use an internal energy equation to compute the internal energy rather than a total energy equation, our scheme does not conserve total energy when the specific kinetic energy is computed from the velocities, i.e., $K_e = \frac{1}{2}u^2$. However we solve an *independent* equation for the specific kinetic energy:

$$\rho \frac{D}{Dt}(K_e) = -u\frac{\partial p}{\partial x} + \frac{\sigma_t}{c}\mathcal{F}_0 u. \tag{6}$$

The solution to this equation is a second-order accurate approximation to the specific kinetic energy, and when this solution is used rather than $\frac{1}{2}u^2$, total energy is conserved. Of course, as the mesh is refined, the specific energy computed with Eq. (6) converges to $\frac{1}{2}u^2$. Thus while our method is not conservative in the usual sense, it is nonetheless conservative.

The radiation transport equation given above and the associated terms coupling it to the hydrodynamics equations represent approximate laboratory-frame equations (as opposed to comoving-frame equations) that are known to be accurate for non-relativistic material velocities and a grey radiation approximation [5]. More specifically, this approximation analytically preserves total mass, momentum, and energy, yields the correct equilibrium solutions to $O(u/c)$, and is correct to $O(u/c)$ in the equilibrium-diffusion limit. Note however, that we have expressed the transport equation in a form that includes the Lagrangian derivative. This is nothing more than an algebraic manipulation of the standard transport equation that facilitates the solution of the transport equation on a moving mesh.

3. The radiation moment equations and the variable Eddington factor

In this section we derive the radiation moment equations and the VEF method. The radiative transfer equations consist of the radiation transport equation and a material temperature equation.

The radiation energy equation is obtained by integrating the transport equation over all directions:

$$\rho \frac{D}{Dt}\left(\frac{\mathcal{E}}{\rho}\right) + \frac{\partial \mathcal{F}}{\partial x} - \frac{\partial}{\partial x}(\mathcal{E}u) + \sigma_a \phi = \sigma_a acT^4 - \frac{\sigma_t}{c}\mathcal{F}_0 u, \tag{7}$$

and the radiation momentum equation is obtained by first multiplying the transport equation by μ/c and then integrating over all directions:

$$\frac{\rho}{c^2}\frac{D}{Dt}\left(\frac{\mathcal{F}}{\rho}\right) + \frac{\partial P}{\partial x} - \frac{\partial}{\partial x}\left(\frac{u}{c}\frac{\mathcal{F}}{c}\right) + \frac{\sigma_t}{c}\mathcal{F}_0 = 0, \tag{8}$$

where P denotes the radiation pressure:

$$P = \frac{1}{c}2\pi \int_{-1}^{+1} \mu^2 \psi \, d\mu. \tag{9}$$

Note that there are two equations and three unknowns, ϕ, $\mathcal{F}$, P. Also note that the hydrodynamics equations only require knowledge of ϕ and $\mathcal{F}$. Therefore, if we can find an exact closure relationship to define P, we can substitute the moment equations for the transport equation and have a complete set of radiation-hydrodynamic equations. The Eddington factor is an exact closure that relates the angle-integrated intensity to pressure:

$$P = f\frac{\phi}{c}, \tag{10}$$

where

$$f = P\frac{c}{\phi} = \frac{2\pi \int_{-1}^{+1} \mu^2 \psi \, d\mu}{2\pi \int_{-1}^{+1} \psi \, d\mu} = \langle \mu^2 \rangle. \tag{11}$$

Of course, it is clear from Eqs. (9) and (10) one cannot compute an exact Eddington factor without knowledge of the angular intensity solution to the transport equation. Nonetheless, one can define an iteration scheme involving the transport equation, the moment equations and the hydrodynamics equations that is far more efficient than solving the radiation-transport equation and the hydrodynamic equations alone. The Variable Eddington Factor method is a classic nonlinear method for accelerating scattering source iterations in S_n neutron transport calculations [1]. The VEF method yields analogous acceleration of the scattering and black-body re-emission sources in radiative transfer calculations. In problems with diffusive regions, acceleration is essential because the unaccelerated number of required transport iterations becomes unbounded as the problem becomes increasingly diffusive, whereas the number of iterations using the VEF method not only remains bounded, but remains relatively small. For instance, consider an infinite homogeneous medium. In the limit as the medium becomes increasingly diffusive, the S_n solution will yield an Eddington factor of one-third with a single iteration, immediately yielding the correct diffusion solution from the moment equations. Thus only one iteration will be required. The success of the VEF method follows from the fact that if S_n source iterations are performed without the VEF method, the Eddington factors converge much more quickly than the scattering sources themselves [6]. Thus our HOLO VEF method achieves high efficiency in two ways. First, the VEF iterations converge quickly, significantly reducing the total number of S_n solves required. Second, in keeping with the theme of a HOLO method, the S_n solves that would otherwise have to be done in the solution of the radiation-hydrodynamics equations are replaced with much less expensive moment equation solves.

4. Overview of the HOLO VEF method

In this section we give a very high-level overview of our HOLO VEF method. The basic iteration scheme is easily explained.

1. Solve the transport equation while lagging the scattering and emission sources.
2. Compute the Eddington factor.
3. Solve the low-order radiation-hydrodynamics equations (moment plus hydrodynamics) using the updated Eddington factor.
4. Use the radiation-hydrodynamics solution to update the scattering and emission sources in the transport equation.
5. Return to 1 and repeat until convergence is achieved.

This represents a straightforward generalization of the classic VEF method, which is applied to the linearized Boltzmann transport equation solved in isolation [7,6]. We later explain the full details of our iteration scheme in Section 5.

Several properties of the VEF method should be noted.

- It is straightforward to invert the transport equation when the scattering and emission sources are lagged for two reasons. First, certain terms in the equation that could complicate the process are treated explicitly in time and thus are effectively known during the iteration process. Second, the transport operator that must be inverted is an advection-reaction equation that has a block lower-triangular structure and can thus be directly inverted using a back-substitution process known as a "sweep" [8].
- The iteration process rapidly converges under nearly all circumstances [1]. Significant negativities in the angular intensities can cause it to diverge, but our discretization schemes, while not monotone, are nonetheless strongly damped and negativities have not been a problem with reasonably resolved meshes. There are established methods for ensuring positive transport solutions given positive sources [9], but we know of no second-order discretizations for the moment equations that are strictly positive. One cannot have a strictly positive solution unless both the transport and moment discretizations are strictly positive.
- It is well known that the spatial discretization used for the transport equation can differ from that used for the moment and hydrodynamic equations without affecting the convergence rate of the iterations [1]. This is a key property that plays a major role in this work.
- The order accuracy of the transport, moment, and hydrodynamic solutions is generally reflected by the order accuracy of the discretization scheme of lowest order used for any set of equations. This follows from the fact that if one contaminates a higher-order equation with lower-order information, one cannot expect a higher-order solution. Thus a lower-order equation in a coupled system of equations can render the overall system solution lower-order accurate. We use second-order discretizations for all of our equations. Thus our overall scheme is second-order accurate, which we later computationally demonstrate.
- It is essential to have a radiation-hydrodynamics discretization that preserves the equilibrium-diffusion limit because those problems often have highly diffusive regions. Multiple works have been published for designing asymptotic-preserving schemes for radiative transfer and radiation-hydrodynamics, such as those using M1 model [10,11]. In [12], asymptotic-preserving schemes for general conservation equations with source terms that have a diffusion limit are described. It has been our experience that any radiative transfer scheme that preserves this limit when applied to pure radiative transfer problems will also preserve it when applied to radiation-hydrodynamics. Asymptotic preservation of diffusion limits can be difficult to achieve for S_n spatial discretizations [13], but when the VEF method is used, diffusion limits can be preserved with almost any S_n discretization as long as the moment equations preserve that limit. More

specifically, the only property required of the discrete S_n equations is that they generate an Eddington factor of 1/3 to leading asymptotic order. Easy preservation of the equilibrium-diffusion limit is another highly desirable property of the VEF method that we exploit. We later computationally demonstrate that our radiation-hydrodynamics scheme is asymptotic-preserving in the equilibrium-diffusion limit.

- The moment equations produce solutions for ϕ and $\mathcal{F}$ that will generally differ from the S_n solutions for those same quantities if independent transport and moment discretizations are used. However, if the discrete transport and moment equations are of the same order of accuracy, then both sets of solutions for ϕ and $\mathcal{F}$ will have the same order accuracy, and the solution sets will converge to each other in the limit as the spatial mesh is refined. The latter property follows from the fact that the analytic transport and moment equations yield the same solutions.
- Our discretization for the moment equations are conservative independent of mesh refinement, which is easy to achieve. However, our S_n solutions for ϕ and $\mathcal{F}$ are generally not conservative except in the limit as the spatial mesh is refined. The latter property is a direct result of using different discretizations for the S_n and moment equations. From our viewpoint, this establishes the moment solutions for ϕ and $\mathcal{F}$ as the "preferred" solutions. Since the moment equations are coupled directly to the hydrodynamic equations, a conservative radiation-hydrodynamics discretization requires conservative moment equations.

5. The TR/BDF2 method

Our method combines a TR/BDF2 time discretization for the radiative transfer and radiation moment equations with a standard second-order predictor-corrector for the Lagrangian hydrodynamics scheme. The properties of the standard TR/BDF2 method are discussed in [2]. A non-standard form of the TR/BDF2 method is used. The non-standard form we use here is equivalent to the standard form, but more easily applied in our method. It was first used in a radiation-hydrodynamics method by Bolding, Hansel, Morel, and Lowrie [14]. Applying this scheme to the following equation:

$$\frac{\partial u}{\partial t} = \mathbf{A}u\,, \tag{12}$$

we obtain

$$\frac{2(u^{n+1/2}-u^n)}{\Delta t_n} = \frac{1}{2}\mathbf{A}^{n+1/2}u^{n+1/2} + \frac{1}{2}\mathbf{A}^n u^n\,, \tag{13a}$$

$$\frac{2(u^{n+1}-u^{n+1/2})}{\Delta t_n} = \frac{2}{3}\mathbf{A}^{n+1}u^{n+1} + \frac{1}{6}\mathbf{A}^{n+1/2}u^{n+1/2} + \frac{1}{6}\mathbf{A}^n u^n\,, \tag{13b}$$

where Δt_n is the time step from t_n to t_{n+1}. Each equation represents a conservation statement over each half time step, respectively, which facilitates coupling of the radiation moment and hydrodynamic equations. We stress however, that if we substituted a standard BDF2 discretization for Eq. (13b), i.e.,

$$3\frac{(u^{n+1}-u^{n+1/2})}{\Delta t_n} = \mathbf{A}^{n+1}u^{n+1} + \frac{(u^{n+1/2}-u^n)}{\Delta t_n}\,, \tag{13c}$$

the solution to Eqs. (13a) and (13c) would be the same as the solution to Eqs. (13a) and (13b). This follows the fact that Eqs. (13a) and (13b) can be linearly combined to obtain Eq. (13c).

6. Iteration scheme and time discretization

The overall iteration scheme is nested with an outer iteration on the variable Eddington factors, and an inner iteration for the solution of the radiation hydrodynamic equations given the Eddington factors. The overall time discretization for the radiation-hydrodynamics equations is of the IMEX (implicit-explicit) type, which enables separation of the solution process into three component solves without loss of second-order accuracy: a purely explicit standard hydro solve, an explicit addition of radiation momentum deposition to the material momentum equation, and an implicit simultaneous solution of the radiation moment equations and an equation for the change in internal energy due to radiation energy deposition and emission. The radiation-hydrodynamic equations are iterated to full nonlinear convergence. All $O(\frac{u}{c})$ terms are treated explicitly during each iteration, but are nonetheless iterated to implicit convergence. In order to reduce the number of transport solves per hydrodynamics solve, we effectively spread the TR/BDF2 solution process over two hydrodynamics solves. More specifically, each time step is partitioned into two half time steps with converged S_n and radiation-hydrodynamics solves over each half step.

The VEF or outer iteration process can be described as follows:

First Half Time Step - Crank-Nicholson

1. Perform one Crank-Nicholson S_n solve using the lagged information from the previous radiation-hydrodynamics solve and compute the VEF's.

2. Using the VEF's from the previous S_n solve, fully solve the radiation-hydrodynamics equations using the Crank-Nicholson method in the implicit portions of the solution process.
3. Return to Step 1 and continue iterating until convergence of the radiation-hydrodynamics solutions.

Second Half Time Step - BDF2

1. Perform one BDF2 S_n solve using the lagged information from the previous radiation-hydrodynamics solve and compute the VEF's.
2. Using the VEF's from the previous S_n solve, fully solve the radiation-hydrodynamics equations using the BDF2 scheme in the implicit portions of the solution process.
3. Return to Step 1 and continue iterating until convergence of the radiation-hydrodynamics solutions.

The outer iteration equations for the first half time step from t_k to $t_{k+1/2}$ are given as follows, where the iteration index is denoted by ℓ:

- S_n Solve

$$\begin{aligned}
&\frac{\rho}{c}\frac{(\psi^{\ell+1/2}/\rho^{\ell})^{k+1/2}-(\psi/\rho)^{k}}{\Delta t/2}\\
&+\frac{1}{2}\{\frac{\partial}{\partial x}(\mu_m\psi^{k+1/2,\ell+1/2}-[\frac{u}{c}\psi]^{k+1/2,\ell})+\sigma_t^{k+1/2,\ell}\psi^{k+1/2,\ell+1/2}\}\\
&+\frac{1}{2}\{\frac{\partial}{\partial x}(\mu_m\psi^{k}-[\frac{u}{c}\psi]^{k})+[\sigma_t\psi]^{k}\}\\
&=\frac{1}{2}\{\frac{1}{4\pi}[\sigma_s c\mathcal{E}]^{k+1/2,\ell}+\frac{1}{4\pi}[\sigma_a acT^4]^{k+1/2,\ell}-\frac{1}{4\pi}[\sigma_t\mathcal{F}_0\frac{u}{c}]^{k+1/2,\ell}\\
&+\frac{\mu_m}{\pi}[\sigma_t\mathcal{E}u]^{k+1/2,\ell}\}\\
&+\frac{1}{2}\{\frac{1}{4\pi}[\sigma_s c\mathcal{E}]^{k}+\frac{1}{4\pi}[\sigma_a acT^4]^{k}-\frac{1}{4\pi}[\sigma_t\mathcal{F}_0\frac{u}{c}]^{k}+\frac{\mu_m}{\pi}[\sigma_t\mathcal{E}u]^{k}\}\,.
\end{aligned}\tag{14}$$

- RH Solve

$$\rho\frac{u^{k+1/2,\ell+1}-u^{k}}{\Delta t/2}=-\frac{\partial p^{k+1/4,\ell+1}}{\partial x}+\frac{1}{2}[\frac{\sigma_t}{c}\mathcal{F}_0]^{k}+\frac{1}{2}[\frac{\sigma_t}{c}\mathcal{F}_0]^{k+1/2,\ell+1}\,,\tag{15}$$

$$\begin{aligned}
\rho\frac{e^{k+1/2,\ell+1}-e^{k}}{\Delta t/2}=&-[p\frac{\partial u}{\partial x}]^{k+1/4,\ell+1}+\frac{1}{2}[\sigma_a c(\mathcal{E}-aT^4)]^{k}\\
&+\frac{1}{2}[\sigma_a c(\mathcal{E}-aT^4)]^{k+1/2,\ell+1}\,,
\end{aligned}\tag{16}$$

$$\begin{aligned}
\rho\frac{(\frac{1}{2}u^2)^{k+1/2,\ell+1}-(\frac{1}{2}u^2)^{k}}{\Delta t/2}=&-[u\frac{\partial p}{\partial x}]^{k+1/4,\ell+1}+\frac{1}{2}[\sigma_t\mathcal{F}_0\frac{u}{c}]^{k}\\
&+\frac{1}{2}[\sigma_t\mathcal{F}_0\frac{u}{c}]^{k+1/2,\ell+1}\,,
\end{aligned}\tag{17}$$

$$\begin{aligned}
&\rho\frac{(\mathcal{E}/\rho)^{k+1/2,\ell+1}-(\mathcal{E}/\rho)^{k}}{\Delta t/2}+\frac{1}{2}\frac{\partial\mathcal{F}^{k+1/2,\ell+1}}{\partial x}+\frac{1}{2}\frac{\partial\mathcal{F}^{k}}{\partial x}\\
&=\frac{1}{2}[\sigma_a c(aT^4-\mathcal{E})]^{k+1/2,\ell+1}+\frac{1}{2}[\sigma_a c(aT^4-\mathcal{E})]^{k}\\
&-\frac{1}{2}[\sigma_t\mathcal{F}_0\frac{u}{c}]^{k+1/2,\ell+1}+\frac{1}{2}\frac{\partial(\mathcal{E}u)^{k+1/2,\ell+1}}{\partial x}\\
&-\frac{1}{2}[\sigma_t\mathcal{F}_0\frac{u}{c}]^{k}+\frac{1}{2}\frac{\partial(\mathcal{E}u)^{k}}{\partial x}\,,
\end{aligned}\tag{18}$$

$$\begin{aligned}
&\frac{\rho}{c^2}\frac{(\mathcal{F}/\rho)^{k+1/2,\ell+1}-(\mathcal{F}/\rho)^{k}}{\Delta t/2}+\frac{1}{2}\frac{\partial(f^{k+1/2,\ell+1/2}\mathcal{E}^{k+1/2,\ell+1})}{\partial x}\\
&+\frac{1}{2}\frac{\partial(f\mathcal{E})^{k}}{\partial x}+\frac{1}{2}[\frac{\sigma_t}{c}\mathcal{F}_0]^{k+1/2,\ell+1}+\frac{1}{2}[\frac{\sigma_t}{c}\mathcal{F}_0]^{k}\\
&-\frac{1}{2}\frac{1}{c^2}\frac{\partial(\mathcal{F}u)^{k+1/2,\ell+1}}{\partial x}-\frac{1}{2}\frac{1}{c^2}\frac{\partial(\mathcal{F}u)^{k}}{\partial x}=0\,.
\end{aligned}\tag{19}$$

Note that a time index for the ρ's appearing before each time derivative need no time index because when volume integrations are performed, in the spatial discretization process, these densities become masses which are constant in time. Note that while many terms are lagged in the S_n solve, only the Eddington factors are lagged in the radiation-hydrodynamics solve. The iterations for the first-half time step are converged before proceeding to the second half time step.

The outer iteration equations for the second half time step from $t_{k+1/2}$ to t_{k+1} are given as follows:

- S_n Solve

$$\begin{aligned}
&\frac{\rho}{c}\frac{(\psi^{\ell+1/2}/\rho^{\ell})^{k+1}-(\psi/\rho)^{k+1/2}}{\Delta t/2}\\
&+\frac{2}{3}\{\frac{\partial}{\partial x}(\mu_m\psi^{k+1,\ell+1/2}-[\frac{u}{c}\psi]^{k+1,\ell})+\sigma_t^{k+1,\ell}\psi^{k+1,\ell+1/2}\}\\
&+\frac{1}{6}\{\frac{\partial}{\partial x}(\mu_m\psi^{k+1/2}-[\frac{u}{c}\psi]^{k+1/2})+[\sigma_t\psi]^{k+1/2}\}\\
&+\frac{1}{6}\{\frac{\partial}{\partial x}(\mu_m\psi^{k}-[\frac{u}{c}\psi]^{k})+[\sigma_t\psi]^{k}\}\\
&=\frac{2}{3}\{\frac{1}{4\pi}[\sigma_s c\mathcal{E}]^{k+1,\ell}+\frac{1}{4\pi}[\sigma_a acT^4]^{k+1,\ell}-\frac{1}{4\pi}[\sigma_t\mathcal{F}_0\frac{u}{c}]^{k+1,\ell}\\
&+\frac{\mu_m}{\pi}[\sigma_t\mathcal{E}u]^{k+1,\ell}\}\\
&+\frac{1}{6}\{\frac{1}{4\pi}[\sigma_s c\mathcal{E}]^{k+1/2}+\frac{1}{4\pi}[\sigma_a acT^4]^{k+1/2}-\frac{1}{4\pi}[\sigma_t\mathcal{F}_0\frac{u}{c}]^{k+1/2}\\
&+\frac{\mu_m}{\pi}[\sigma_t\mathcal{E}u]^{k+1/2}\}\\
&+\frac{1}{6}\{\frac{1}{4\pi}[\sigma_s c\mathcal{E}]^{k}+\frac{1}{4\pi}[\sigma_a acT^4]^{k}-\frac{1}{4\pi}[\sigma_t\mathcal{F}_0\frac{u}{c}]^{k}+\frac{\mu_m}{\pi}[\sigma_t\mathcal{E}u]^{k}\}\,.
\end{aligned}\tag{20}$$

- RH Solve

$$\begin{aligned}
\rho\frac{u^{k+1,\ell+1}-u^{k+1/2}}{\Delta t/2}=&-\frac{\partial p^{k+3/4,\ell+1}}{\partial x}+\frac{1}{6}[\frac{\sigma_t}{c}\mathcal{F}_0]^{k}\\
&+\frac{1}{6}[\frac{\sigma_t}{c}\mathcal{F}_0]^{k+1/2}+\frac{2}{3}[\frac{\sigma_t}{c}\mathcal{F}_0]^{k+1,\ell+1}\,,
\end{aligned}\tag{21}$$

$$\begin{aligned}
\rho\frac{e^{k+1,\ell+1}-e^{k+1/2}}{\Delta t/2}=&-[p\frac{\partial u}{\partial x}]^{k+3/4,\ell+1}+\frac{1}{6}[\sigma_a c(\mathcal{E}-aT^4)]^{k}\\
&+\frac{1}{6}[\sigma_a c(\mathcal{E}-aT^4)]^{k+1/2}\\
&+\frac{2}{3}[\sigma_a c(\mathcal{E}-aT^4)]^{k+1,\ell+1}\,,
\end{aligned}\tag{22}$$

$$\begin{aligned}
\rho\frac{(\frac{1}{2}u^2)^{k+1,\ell+1}-(\frac{1}{2}u^2)^{k+1/2}}{\Delta t/2}=&-[u\frac{\partial p}{\partial x}]^{k+3/4,\ell+1}\\
&+\frac{1}{6}[\sigma_t\mathcal{F}_0\frac{u}{c}]^{k}+\frac{1}{6}[\sigma_t\mathcal{F}_0\frac{u}{c}]^{k+1/2}\\
&+\frac{2}{3}[\sigma_t\mathcal{F}_0\frac{u}{c}]^{k+1,\ell+1}\,,
\end{aligned}\tag{23}$$

$$\begin{aligned}
&\rho\frac{(\mathcal{E}/\rho)^{k+1,\ell+1}-(\mathcal{E}/\rho)^{k+1/2}}{\Delta t/2}+\frac{2}{3}\frac{\partial\mathcal{F}^{k+1,\ell+1}}{\partial x}+\frac{1}{6}\frac{\partial\mathcal{F}^{k+1/2}}{\partial x}+\frac{1}{6}\frac{\partial\mathcal{F}^{k}}{\partial x}\\
&=\frac{2}{3}[\sigma_a c(aT^4-\mathcal{E})]^{k+1,\ell+1}+\frac{1}{6}[\sigma_a c(aT^4-\mathcal{E})]^{k+1/2}+\frac{1}{6}[\sigma_a c(aT^4-\mathcal{E})]^{k}\\
&-\frac{2}{3}[\sigma_t\mathcal{F}_0\frac{u}{c}]^{k+1,\ell+1}-\frac{1}{6}[\sigma_t\mathcal{F}_0\frac{u}{c}]^{k+1/2}-\frac{1}{6}[\sigma_t\mathcal{F}_0\frac{u}{c}]^{k}\\
&+\frac{2}{3}\frac{\partial(\mathcal{E}u)^{k+1,\ell+1}}{\partial x}+\frac{1}{6}\frac{\partial(\mathcal{E}u)^{k+1/2}}{\partial x}+\frac{1}{6}\frac{\partial(\mathcal{E}u)^{k}}{\partial x}\,,
\end{aligned}\tag{24}$$

$$
\begin{aligned}
&\frac{\rho}{c^2}\frac{(\mathcal{F}/\rho)^{k+1,\ell+1}-(\mathcal{F}/\rho)^{k+1/2}}{\Delta t/2}\\
&+\frac{2}{3}\frac{\partial(f^{k+1,\ell+1/2}\mathcal{E}^{k+1,\ell+1})}{\partial x}+\frac{1}{6}\frac{\partial(f\mathcal{E})^{k+1/2}}{\partial x}+\frac{1}{6}\frac{\partial(f\mathcal{E})^{k}}{\partial x}\\
&+\frac{2}{3}[\frac{\sigma_t}{c}\mathcal{F}_0]^{k+1,\ell+1}+\frac{1}{6}[\frac{\sigma_t}{c}\mathcal{F}_0]^{k+1/2}+\frac{1}{6}[\frac{\sigma_t}{c}\mathcal{F}_0]^{k}\\
&-\frac{2}{3}\frac{1}{c^2}\frac{\partial(\mathcal{F}u)^{k+1,\ell+1}}{\partial x}-\frac{1}{6}\frac{1}{c^2}\frac{\partial(\mathcal{F}u)^{k+1/2}}{\partial x}-\frac{1}{6}\frac{1}{c^2}\frac{\partial(\mathcal{F}u)^{k}}{\partial x}=0\,.
\end{aligned}
\tag{25}
$$

The inner iterations are performed to solve the radiation-hydrodynamic equations after the VEF's have been defined by the transport solve. The VEF's are constant during the inner iteration process and thus do not carry an inner iteration index. They could be assigned an outer iteration index, but we prefer to avoid the use of separate symbols for the outer and inner iteration indices. The inner iterations for the first half time step are as follows.

- RH Predictor:

$$
\rho\frac{u^{k+1/4,\ell+1}-u^{k}}{\Delta t/4}=-\frac{\partial p^{k}}{\partial x}+[\frac{\sigma_t}{c}\mathcal{F}_0]^{k+1/4,\ell}\,,
\tag{26}
$$

$$
\rho\frac{e^{k+1/4,\ell+1}-e^{k}}{\Delta t/4}=-[p\frac{\partial u}{\partial x}]^{k}+\sigma_a^{k+1/4,\ell}c(\mathcal{E}-aT^4)^{k+1/4,\ell+1}\,,
\tag{27}
$$

$$
\rho\frac{(\frac{1}{2}u^2)^{k+1/4,\ell+1}-(\frac{1}{2}u^2)^{k}}{\Delta t/4}=-[u\frac{\partial p}{\partial x}]^{k}+\frac{\sigma_t^{k+1/4,\ell}}{c}\mathcal{F}_0^{k+1/4,l}u^{k+1/4,\ell+1}\,,
\tag{28}
$$

$$
\begin{aligned}
&\rho\frac{(\mathcal{E}/\rho)^{k+1/4,\ell+1}-(\mathcal{E}/\rho)^{k}}{\Delta t/4}+\frac{\partial\mathcal{F}^{k+1/4,\ell+1}}{\partial x}\\
&=\sigma_a^{k+1/4,\ell}c(aT^4-\mathcal{E})^{k+1/4,\ell+1}\\
&-\frac{\sigma_t^{k+1/4,\ell}}{c}\mathcal{F}_0^{k+1/4,l}u^{k+1/4,\ell+1}+\frac{\partial(\mathcal{E}^{k+1/4,l}u^{k+1/4,\ell+1})}{\partial x}\,,
\end{aligned}
\tag{29}
$$

$$
\begin{aligned}
&\frac{\rho}{c^2}\frac{(\mathcal{F}/\rho)^{k+1/4,\ell+1}-(\mathcal{F}/\rho)^{k}}{\Delta_t/4}+\frac{\partial(f^{k+1/4,\ell+1/2}\mathcal{E}^{k+1/4,\ell+1})}{\partial x}\\
&\quad+\frac{\sigma_t^{k+1/4,\ell}}{c}\mathcal{F}_0^{k+1/4,\ell+1}-\frac{1}{c^2}\frac{\partial(\mathcal{F}^{k+1/4,l}u^{k+1/4,\ell+1})}{\partial x}=0\,.
\end{aligned}
\tag{30}
$$

- RH Corrector:

$$
\rho\frac{u^{k+1/2,\ell+1}-u^{k}}{\Delta t/2}=-\frac{\partial p^{k+1/4,\ell+1}}{\partial x}+\frac{1}{2}[\frac{\sigma_t}{c}\mathcal{F}_0]^{k}+\frac{1}{2}[\frac{\sigma_t}{c}\mathcal{F}_0]^{k+1/2,\ell}\,,
\tag{31}
$$

$$
\begin{aligned}
\rho\frac{e^{k+1/2,\ell+1}-e^{k}}{\Delta t/2}=&-[p\frac{\partial u}{\partial x}]^{k+1/4,\ell+1}+\frac{1}{2}[\sigma_a c(\mathcal{E}-aT^4)]^{k}\\
&+\frac{1}{2}\sigma_a^{k+1/2,\ell}c(\mathcal{E}-aT^4)^{k+1/2,\ell+1}\,,
\end{aligned}
\tag{32}
$$

$$
\begin{aligned}
\rho\frac{(\frac{1}{2}u^2)^{k+1/2,\ell+1}-(\frac{1}{2}u^2)^{k}}{\Delta t/2}=&-[u\frac{\partial p}{\partial x}]^{k+1/4,\ell+1}+\frac{1}{2}[\frac{\sigma_t}{c}\mathcal{F}_0u]^{k}\\
&+\frac{1}{2}\frac{\sigma_t^{k+1/2,l}}{c}\mathcal{F}_0^{k+1/2,\ell}u^{k+1/2,\ell+1}\,,
\end{aligned}
\tag{33}
$$

$$
\begin{aligned}
&\rho\frac{(\mathcal{E}/\rho)^{k+1/2,\ell+1}-(\mathcal{E}/\rho)^{k}}{\Delta t/2}+\frac{1}{2}\frac{\partial\mathcal{F}^{n+1/2,\ell+1}}{\partial x}+\frac{1}{2}\frac{\partial\mathcal{F}^{n}}{\partial x}\\
&=\frac{1}{2}\sigma_a^{k+1/2,\ell}c(aT^4-\mathcal{E})^{k+1/2,\ell+1}+\frac{1}{2}[\sigma_a c(aT^4-\mathcal{E})]^{k}\\
&-\frac{1}{2}\frac{\sigma_t^{k+1/2,\ell}}{c}\mathcal{F}_0^{k+1/2,l}u^{k+1/2,\ell+1}+\frac{1}{2}\frac{\partial(\mathcal{E}^{k+1/2,\ell}u^{k+1/2,\ell+1})}{\partial x}\\
&-\frac{1}{2}[\frac{\sigma_t}{c}\mathcal{F}_0u]^{k}+\frac{1}{2}\frac{\partial(\mathcal{E}u)^{k}}{\partial x}\,,
\end{aligned}
\tag{34}
$$

$$\frac{\rho}{c^2}\frac{(\mathcal{F}/\rho)^{k+1/2,\ell+1}-(\mathcal{F}/\rho)^{k}}{\Delta t/2}+\frac{1}{2}\frac{\partial(f^{k+1/2,\ell+1/2}\mathcal{E}^{k+1/2,\ell+1})}{\partial x}+\frac{1}{2}\frac{\partial(f\mathcal{E})^{k}}{\partial x}$$
$$+\frac{1}{2}\frac{\sigma_t^{k+1/2,\ell}}{c}\mathcal{F}_0^{k+1/2,\ell+1}+\frac{1}{2}[\frac{\sigma_t}{c}\mathcal{F}_0]^{k} \tag{35}$$
$$-\frac{1}{2}\frac{1}{c^2}\frac{\partial(\mathcal{F}^{k+1/2,\ell}u^{k+1/2,l+1})}{\partial x}-\frac{1}{2}\frac{1}{c^2}\frac{\partial(\mathcal{F}u)^{k}}{\partial x}=0\,.$$

The inner iterations for the second half time step are as follows.

- RH Predictor:

$$\rho\frac{u^{k+3/4,\ell+1}-u^{k+1/2}}{\Delta t/4}=-\frac{\partial p^{k+1/2}}{\partial x}+(\frac{\sigma_t}{c}\mathcal{F}_0)^{k+3/4,\ell}\,, \tag{36}$$

$$\rho\frac{e^{k+3/4,\ell+1}-e^{k+1/2}}{\Delta t/4}=-[p\frac{\partial u}{\partial x}]^{k+1/2}+\sigma_a^{k+3/4,\ell}c(\mathcal{E}-aT^4)^{k+3/4,\ell+1}\,, \tag{37}$$

$$\rho\frac{(\frac{1}{2}u^2)^{k+3/4,\ell+1}-(\frac{1}{2}u^2)^{k+1/2}}{\Delta t/4}=-[u\frac{\partial p}{\partial x}]^{k+1/2}+\frac{\sigma_t^{k+3/4,\ell}}{c}\mathcal{F}_0^{k+3/4,\ell}u^{k+3/4,\ell+1}\,, \tag{38}$$

$$\rho\frac{(\mathcal{E}/\rho)^{k+3/4,\ell+1}-(\mathcal{E}/\rho)^{k+1/2}}{\Delta t/4}+\frac{\partial\mathcal{F}^{k+3/4,\ell+1}}{\partial x}$$
$$=\sigma_a^{k+3/4,\ell}c(aT^4-\mathcal{E})^{k+3/4.\ell+1}$$
$$-\frac{\sigma_t^{k+3/4,\ell}}{c}\mathcal{F}_0^{k+3/4,\ell}u^{k+3/4,\ell+1}+\frac{\partial(\mathcal{E}^{k+3/4,\ell}u^{k+3/4,\ell+1})}{\partial x}\,, \tag{39}$$

$$\frac{\rho}{c^2}\frac{(\mathcal{F}/\rho)^{k+3/4,\ell+1}-(\mathcal{F}/\rho)^{k+1/2}}{\Delta_t/4}+\frac{\partial(f^{k+3/4,\ell+1/2}\mathcal{E}^{k+3/4,\ell+1})}{\partial x}$$
$$+\frac{\sigma_t^{k+3/4,\ell}}{c}\mathcal{F}_0^{k+3/4,\ell+1}-\frac{1}{c^2}\frac{\partial(\mathcal{F}^{k+3/4,\ell}u^{k+3/4,\ell+1})}{\partial x}=0\,. \tag{40}$$

- RH Corrector:

$$\rho\frac{u^{k+1,\ell+1}-u^{k+1/2}}{\Delta t/2}=-\frac{\partial p^{k+3/4,\ell+1}}{\partial x}+\frac{1}{6}[\frac{\sigma_t}{c}\mathcal{F}_0]^{k}$$
$$+\frac{1}{6}[\frac{\sigma_t}{c}\mathcal{F}_0]^{k+1/2}+\frac{2}{3}[\frac{\sigma_t}{c}\mathcal{F}_0]^{k+1,\ell}\,, \tag{41}$$

$$\rho\frac{e^{k+1,\ell+1}-e^{k+1/2}}{\Delta t/2}=-[p\frac{\partial u}{\partial x}]^{k+3/4,\ell+1}+\frac{1}{6}[\sigma_a c(\mathcal{E}-aT^4)]^{k}$$
$$+\frac{1}{6}[\sigma_a c(\mathcal{E}-aT^4)]^{k+1/2}$$
$$+\frac{2}{3}\sigma_a^{k+1,\ell}c(\mathcal{E}-aT^4)^{k+1,\ell+1}\,, \tag{42}$$

$$\rho\frac{(\frac{1}{2}u^2)^{k+1,\ell+1}-(\frac{1}{2}u^2)^{k+1/2}}{\Delta t/2}=-[u\frac{\partial p}{\partial x}]^{k+3/4,\ell+1}$$
$$+\frac{1}{6}[\frac{\sigma_t}{c}\mathcal{F}_0u]^{k}+\frac{1}{6}[\frac{\sigma_t}{c}\mathcal{F}_0u]^{k+1/2}$$
$$+\frac{2}{3}\frac{\sigma_t^{k+1,\ell}}{c}\mathcal{F}_0^{k+1,\ell}u^{k+1,\ell+1}\,, \tag{43}$$

$$
\begin{aligned}
&\rho\frac{(\mathcal{E}/\rho)^{k+1,\ell+1}-(\mathcal{E}/\rho)^{k+1/2}}{\Delta t/2}+\frac{2}{3}\frac{\partial\mathcal{F}^{n+1,\ell+1}}{\partial x}+\frac{1}{6}\frac{\partial\mathcal{F}^{k+1/2}}{\partial x}+\frac{1}{6}\frac{\partial\mathcal{F}^{k}}{\partial x}\\
&=\frac{2}{3}\sigma_a^{k+1,\ell}c(aT^4-\mathcal{E})^{k+1,\ell+1}\\
&+\frac{1}{6}[\sigma_a c(aT^4-\mathcal{E})]^{k+1/2}+\frac{1}{6}[\sigma_a c(aT^4-\mathcal{E})]^{k}\\
&-\frac{2}{3}\frac{\sigma_t^{k+1,\ell}}{c}\mathcal{F}_0^{k+1,\ell}u^{k+1,\ell+1}-\frac{1}{6}[\frac{\sigma_t}{c}\mathcal{F}_0u]^{k+1/2}-\frac{1}{6}[\frac{\sigma_t}{c}\mathcal{F}_0u]^{k}\\
&+\frac{2}{3}\frac{\partial(\mathcal{E}^{k+1,\ell}u^{k+1,\ell+1})}{\partial x}+\frac{1}{6}\frac{\partial(\mathcal{E}u)^{k+1/2}}{\partial x}+\frac{1}{6}\frac{\partial(\mathcal{E}u)^{k}}{\partial x},
\end{aligned}
\tag{44}
$$

$$
\begin{aligned}
&\frac{\rho}{c^2}\frac{(\mathcal{F}/\rho)^{k+1,\ell+1}-(\mathcal{F}/\rho)^{k+1/2}}{\Delta t/2}\\
&+\frac{2}{3}\frac{\partial(f^{k+1,\ell+1/2}\mathcal{E}^{k+1,\ell+1})}{\partial x}+\frac{1}{6}\frac{\partial(f\mathcal{E})^{k+1/2}}{\partial x}+\frac{1}{6}\frac{\partial(f\mathcal{E})^{k}}{\partial x}\\
&+\frac{2}{3}\frac{\sigma_t^{k+1,\ell}}{c}\mathcal{F}_0^{k+1,\ell+1}+\frac{1}{6}[\frac{\sigma_t}{c}\mathcal{F}_0]^{k+1/2}+\frac{1}{6}[\frac{\sigma_t}{c}\mathcal{F}_0]^{k}\\
&-\frac{2}{3}\frac{1}{c^2}\frac{\partial(\mathcal{F}^{k+1,\ell}u^{k+1,\ell+1})}{\partial x}-\frac{1}{6}\frac{1}{c^2}\frac{\partial(\mathcal{F}u)^{k+1/2}}{\partial x}-\frac{1}{6}\frac{1}{c^2}\frac{\partial(\mathcal{F}u)^{k}}{\partial x}=0.
\end{aligned}
\tag{45}
$$

7. Lumped linear discontinuous Galerkin S_N

The spatial domain is discretized into I cells, and the angular domain is discretized into N cells. The spatial index is i, and the angular index is m. Cell centers carry integral indices, and cell edges carry half-integral indices. Each angular cell is characterized by a direction cosine, μ_m, and a quadrature weight, w_m. The S_n angular discretization simply corresponds to collocation at the quadrature points with angular integration via the quadrature set [8]. The spatial dependence of the angular intensity in direction m within cell i is linear and defined in terms of two discrete unknowns, $\psi_{i,m,L}$ and $\psi_{i,m,R}$:

This dependence is given by

$$
\psi_{i,m}(x)=\psi_{i,m,L}B_{i,L}(x)+\psi_{i,m,R}B_{i,R}(x),\quad x\in(x_{i-1/2},x_{i+1/2}),
\tag{46}
$$

where the LLDG basis functions are defined as:

$$
B_{i,L}(x)=\begin{cases}\frac{x_{i+1/2}-x}{x_{i+1/2}-x_{i-1/2}},\ x\in[x_{i-1/2},x_{i+1/2}]\\ 0,\ \text{otherwise}\end{cases},
\tag{47a}
$$

$$
B_{i,R}(x)=\begin{cases}\frac{x-x_{i-1/2}}{x_{i+1/2}-x_{i-1/2}},\ x\in[x_{i-1/2},x_{i+1/2}]\\ 0,\ \text{otherwise}\end{cases}.
\tag{47b}
$$

The cell centered angular intensity is the average of the left and right discontinuous interior-edge intensities:

$$
\psi_{i,m}=\frac{1}{2}(\psi_{i,m,L}+\psi_{i,m,R}).
\tag{48}
$$

The interface or cell-edge intensities are uniquely defined in terms of the interior-edge intensities by upwinding:

$$
\psi_{i-1/2,m}(x)=\begin{cases}\psi_{i-1,m,R}, & \mu_m>0\\ \psi_{i,m,L}, & \mu_m<0\end{cases},
\tag{49a}
$$

$$
\psi_{i+1/2,m}(x)=\begin{cases}\psi_{i,m,R}, & \mu_m>0\\ \psi_{i+1,m,L}, & \mu_m<0\end{cases}.
\tag{49b}
$$

This dependence is illustrated in Fig. 1. Lumping is achieved by using trapezoidal quadrature rather than Gauss quadrature for the FEM weighted residual process.

8. Mixed finite-element method for low order system

MFEM method is applied to the lower order system. The angle-integrated intensities, mass densities, material internal energies, material pressures, and temperatures are piecewise-constant, material velocities and kinetic energies are piecewise-linear. The radiative flux trial space is linear within each cell and formally discontinuous across cell interfaces, but continuity

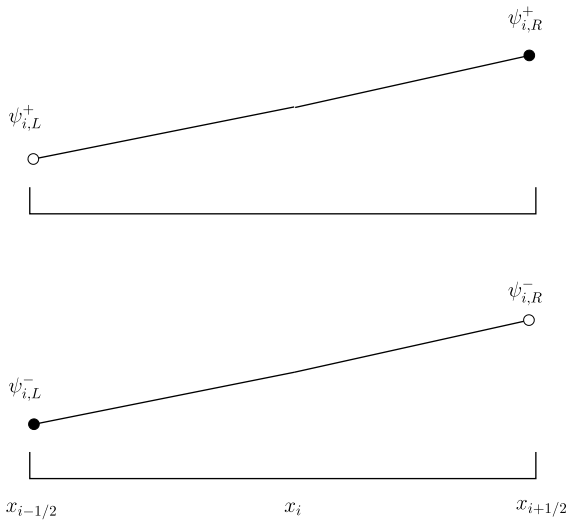

Fig. 1. The spatial dependence of angular intensity for direction m within cell i. The superscript $+$ and $-$ indicate the radiation angular intensity for $\mu_m > 0$ and $\mu_m < 0$, respectively.

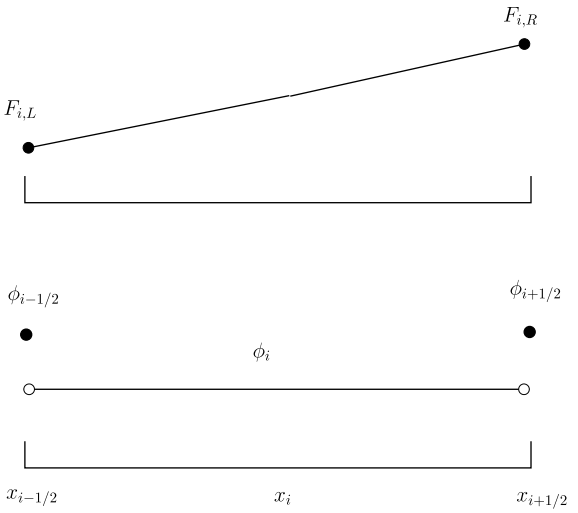

Fig. 2. The spatial dependence of the radiative unknowns within a MFEM cell.

of the fluxes is imposed via cell-edge intensities. The spatial dependence of the radiative unknowns within cell i in the MFEM method is plotted in Fig. 2.

The directionally-integrated radiation intensity is constant within a cell with discontinuous jumps at the cell edges. In other words,

$$\phi_i(x) = \begin{cases} \phi_i, \ x \in (x_{i-1/2}, x_{i+1/2}) \\ \phi_{i\pm1/2}, x = x_{i\pm1/2} \\ 0, \ \text{otherwise} \end{cases} . \tag{50}$$

Since the LLDG and MFEM approximations use the same spatial grid, the Eddington factors are available at any space point as required for the MFEM equations.

The radiative flux, $F_i(x)$, is a piecewise linear function defined by

$$\mathcal{F}_i(x) = \mathcal{F}_{i,L} B_{i,L}(x) + \mathcal{F}_{i,R} B_{i,R}(x) , \tag{51}$$

where $\mathcal{F}_{i,L}$ and $\mathcal{F}_{i,R}$ are the radiative fluxes on the left and right edges of the cell i, respectively, and the basis functions are the same as the ones defined by Eqs. (47a) and (47b) for the LLDG S_n discretization. It is important to note that we have cast the MFEM equations in a hybridized form. In particular, we assume a piecewise linear-discontinuous dependence

for the radiation fluxes together with a piecewise-constant dependence for the intensities with uniquely defined jumps on the cell interfaces. The cell-edge intensities are actually chosen to make the fluxes continuous across the cell interfaces. The alternative is to leave the cell-edge intensities undefined and assume a piecewise linear-continuous dependence for the radiation fluxes. The advantage of the hybridized approach is that one can locally eliminate the fluxes from the system of equations resulting in a reduced SPD system consisting of the cell-center and cell-edge intensities. It is also possible to locally eliminate the cell-center intensities, resulting in an SPD system for the cell-edge intensities. If one does not use the hybridized approach, the radiation fluxes cannot be locally eliminated and one must solve a saddle-point problem.

9. Computational results

9.1. Method of manufactured solutions

The Method of Manufactured Solutions (MMS) was used to test the time and spatial accuracy of our HOLO VEF scheme as the time step and cell width are decreased. The solutions are defined as follows:

$$\rho = Ce^{Ax}, \tag{52}$$

$$u = De^{-Ax+Bt}, \tag{53}$$

$$p = Ee^{Fx+Gt}, \tag{54}$$

$$I = \frac{1}{4\pi} Pe^{Mx+Nt}[c + (4u - \frac{cM}{\sigma_t})\mu], \tag{55}$$

$$\mathcal{E} = Pe^{Mx+Nt}, \tag{56}$$

$$\mathcal{F} = -\frac{c}{3\sigma_t} PMe^{Mx+Nt} + \frac{4u}{3} Pe^{Mx+Nt}. \tag{57}$$

Then, the internal energy and temperature can be expressed as:

$$e = \frac{p}{(\gamma-1)\rho} = \frac{E}{C(\gamma-1)} e^{(F-A)x+Gt}, \tag{58}$$

$$T = \frac{e}{Cv} = \frac{E}{C(\gamma-1)C_v} e^{(F-A)x+Gt}. \tag{59}$$

The corresponding distributed sources are as follows:

$$Q_\rho = 0, \tag{60}$$

$$Q_u = BCDe^{Bt} - ACD^2 e^{-Ax+2Bt} + EFe^{Fx+Gt} + \frac{P}{3} Me^{Mx+Nt}, \tag{61}$$

$$\begin{aligned} Q_e =& \frac{EG}{(\gamma-1)} e^{Fx+Gt} + (\frac{DE(F-A)}{\gamma-1} - ADE) e^{(F-A)x+(G+B)t} \\ & - \sigma_a c[Pe^{Mx+Nt} - \frac{aE^4}{[C(\gamma-1)C_v]^4)} e^{4(F-A)x+4Gt}], \end{aligned} \tag{62}$$

$$\begin{aligned} Q_{\frac{1}{2}u^2} =& BCD^2 e^{-Ax+2Bx} - ACD^3 e^{-2Ax+3Bt} \\ & + DEFe^{(F-A)x+(G+B)t} + \frac{1}{3} DPMe^{(M-A)x+(N+B)t}, \end{aligned} \tag{63}$$

$$\begin{aligned} Q_I =& \frac{1}{4\pi} Pe^{Mx+Nt}\{N(1 - \frac{M}{\sigma_t}\mu) - c\frac{MM}{\sigma_t}\mu^2\} \\ & + \frac{1}{4\pi} PDe^{(M-A)x+(N+B)t}\{\frac{4}{c}(N+B)\mu + 4\mu\mu(M-A) - \frac{M}{3}\} \\ & + \frac{\sigma_a c}{4\pi}(Pe^{Mx+Nt} - aT^4), \end{aligned} \tag{64}$$

$$\begin{aligned} Q_\mathcal{E} =& PNe^{Mx+Nt} + (\sigma_a cP - \frac{c}{3\sigma_t} PMM) e^{Mx+Nt} \\ & + [\frac{4}{3} PD(M-A) - \frac{1}{3} PMD] e^{(M-A)x+(B+N)t} \\ & - \sigma_a c \frac{aE^4}{[C(\gamma-1)C_v]^4)} e^{4(F-A)x+4Gt}, \end{aligned} \tag{65}$$

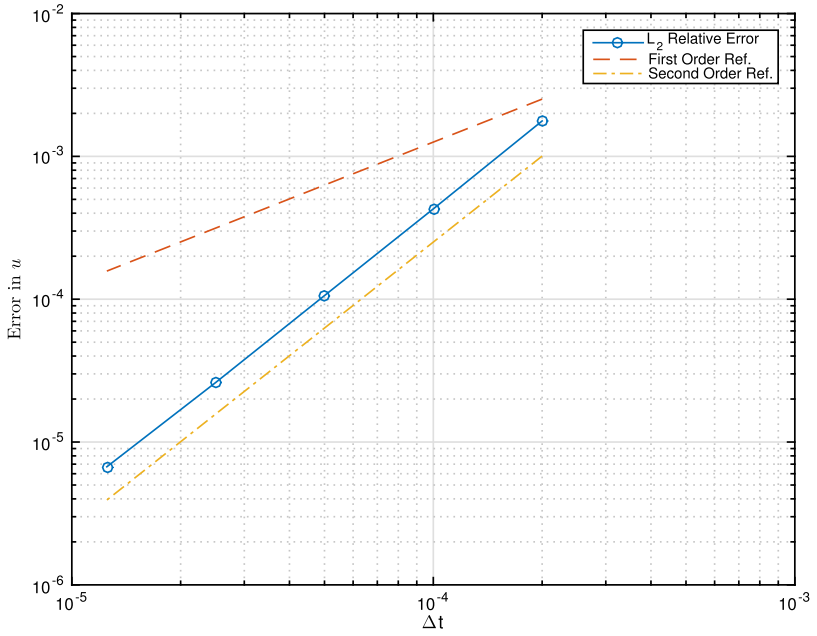

Fig. 3. Convergence in time and space of velocities for MMS problem.

$$Q_F = -\frac{1}{3c\sigma_t} PMNe^{Mx+Nt} + \frac{4}{3c^2} PD(B+N)e^{(M-A)x+(B+N)t} . \tag{66}$$

The constants were chosen as $A = -1$, $B = D = E = F = G = M = N = 1$, and $\sigma_t = \sigma_a = 1$ cm^{-1}. The calculation was performed for a slab with an initial spatial domain of $[0, 1]$ cm. The S_n calculations for this problem were performed with Gauss S8 quadrature. The calculation was terminated at $t = 10^{-3}$ sh. The time steps and cell widths for each problem were given by $2 \times 10^{-4} \times (\frac{1}{2})^n$ sh and $0.2 \times (\frac{1}{2})^n$ cm for $n = (0, 1, 2, \cdots, 4)$. Thus we performed a series of calculations in which the time steps and spatial cell widths were simultaneously reduced by a factor of 2 for each successive calculation. The L_2 errors between the numerical and analytical solutions for u, e, $\mathcal{E}$ and $\mathcal{F}$ are plotted in Figs. 3 to 6. It can be seen from the reference second-order lines that the solutions are second-order accurate in time and space. The energy balance is defined as:

$$\text{Balance} = 1 - \frac{\text{total energy} + \text{integrated radiation leakage and source}}{\text{initial total energy}} , \tag{67}$$

where the total energy is the summation of kinetic energy, internal energy and radiation energy, as plotted in Fig. 7. The kinetic energy, internal energy, radiation energy and total energy as a function of time are also plotted in Fig. 8. The energy balance is plotted in Fig. 9. The balance is essentially zero to round-off as a function of time, which indicates the expected conservation.

9.2. Thick diffusion limit

Our HOLO VEF method was also tested in the thick diffusion limit for different values of the asymptotic scaling parameter, ϵ, using manufactured solutions [15]. The time derivative, cross sections, material velocity, and source associated with the radiation were scaled as follows [16]:

$$\begin{aligned} \frac{d}{dt} &\to \epsilon \frac{d}{dt} , \\ \sigma_t &\to \frac{\sigma_t}{\epsilon} , \\ \sigma_a &\to \frac{\sigma_t}{\epsilon} - \sigma_s , \\ u &\to u\epsilon , \\ Q &\to Q\epsilon . \end{aligned} \tag{68}$$

A detailed asymptotic analysis can be found in reference [17]. The manufactured solutions were defined as follows:

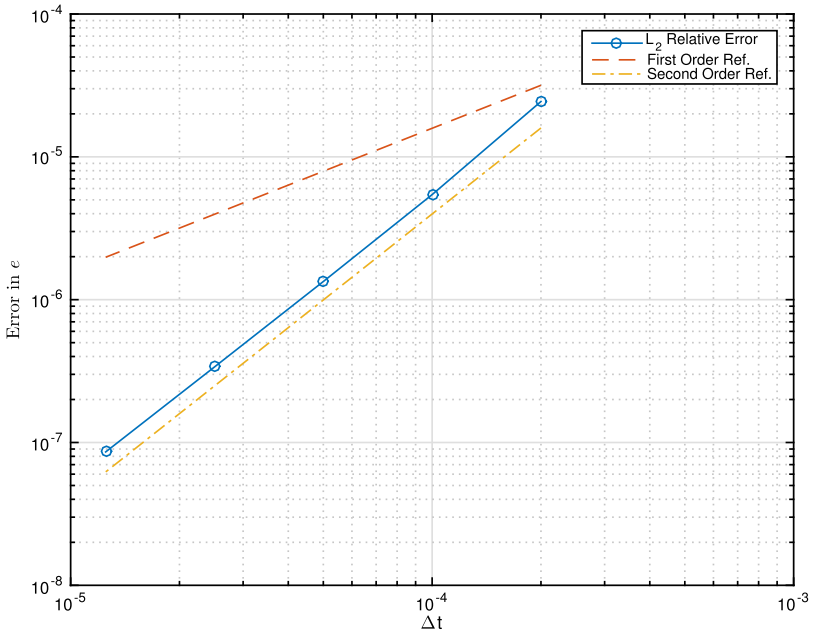

Fig. 4. Convergence in time and space of internal energy for MMS problem.

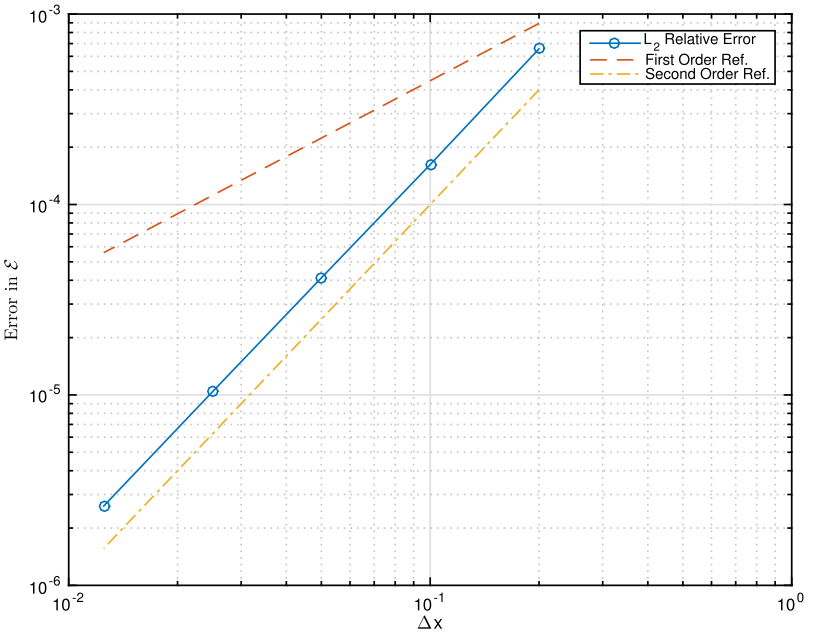

Fig. 5. Convergence in time and space of radiation energy density for MMS problem.

$$\rho = \frac{1}{x^2+1}, \tag{69}$$

$$u = (x^2+1), \tag{70}$$

$$P = (x^2+1), \tag{71}$$

$$\psi = \frac{1}{4\pi} acT^4 \left(\frac{1}{2} + 3\mu + \frac{3}{2}\mu^2\right). \tag{72}$$

We set $\sigma_t = \sigma_a = 1\ cm$, $C_v = 1\ j/cm^3 - keV$ and $\gamma = 2$. The time step was chosen as $1 \times 10^{-5}\ sh$, and the calculation was terminated at t=$4 \times 10^{-4}\ sh$. The initial spatial domain was $[0, 1]\ cm$, divided into 40 cells. The value of ϵ was chosen

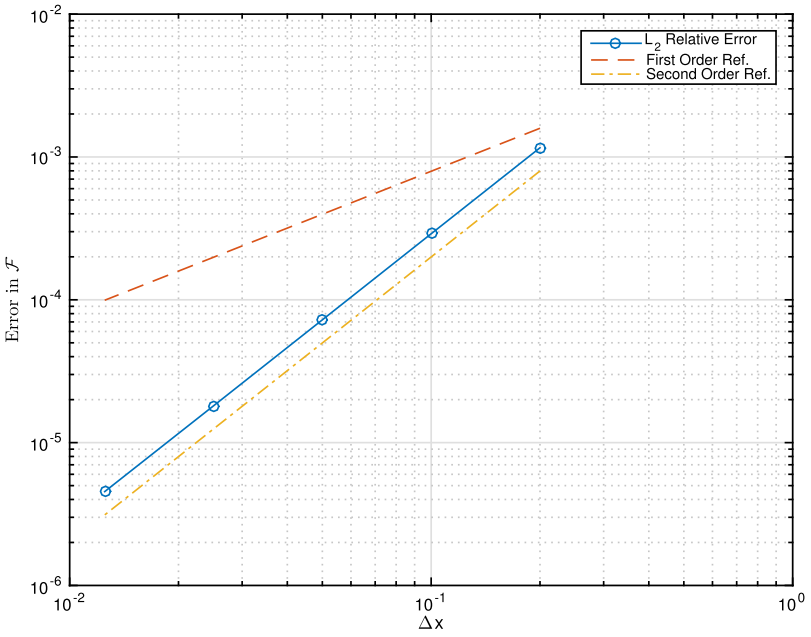

Fig. 6. Convergence in time and space of radiation flux density for MMS problem.

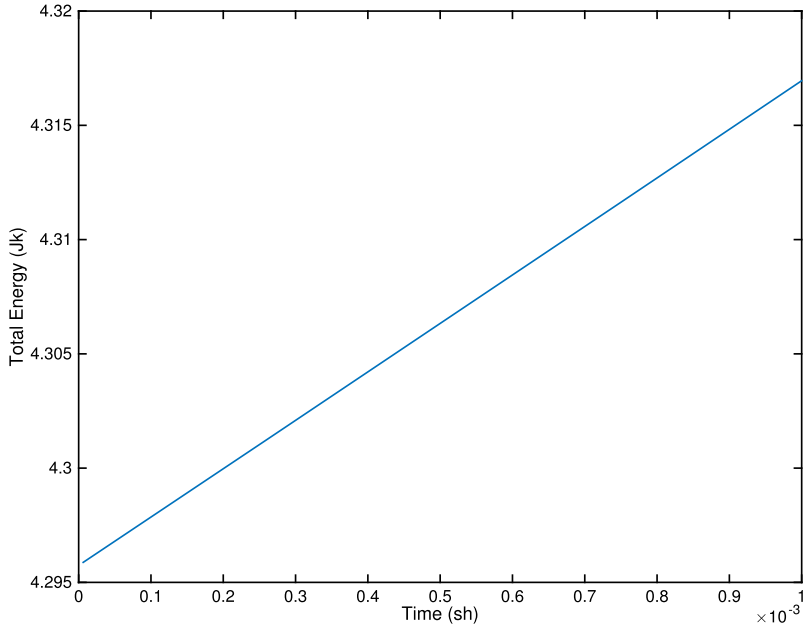

Fig. 7. Total energy as a function of time for MMS problem.

as 1, 0.1 and 0.01. The HOLO VEF solutions for the material temperature and radiation energy density are compared with the analytic equilibrium diffusion solutions in Fig. 10 and 11, respectively.

The results show that the HOLO VEF solution is converging to the diffusion solution as $\epsilon \to 0$, which indicates our HOLO VEF method preserves the thick diffusion limit.

9.3. The radiative shock problem

We also tested our method for two shock problems similar to the ones in [18]. For both shock problems, we set $\gamma = 5/3$, $C_v = 0.14472799784454$ Jk keV^{-1}g^{-1}, and $\sigma_t = \sigma_a = 577.35$ cm^{-1}. The initial conditions for pre- and post-shock regions for $M_0 = 1.2$ and $M_0 = 3$ are listed in Table 1 and 2, respectively.

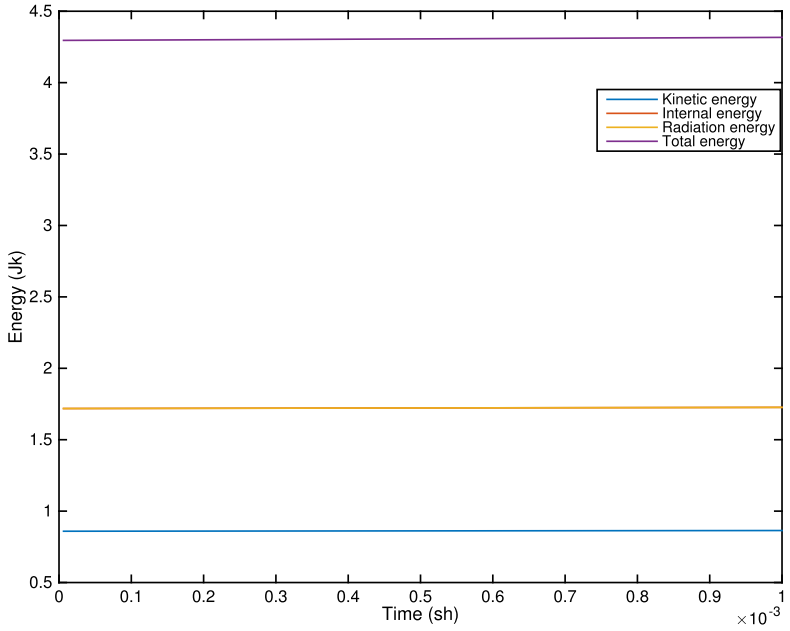

Fig. 8. Kinetic energy, internal energy, radiation energy and total energy as a function of time for MMS problem. (For interpretation of the colors in the figure(s), the reader is referred to the web version of this article.)

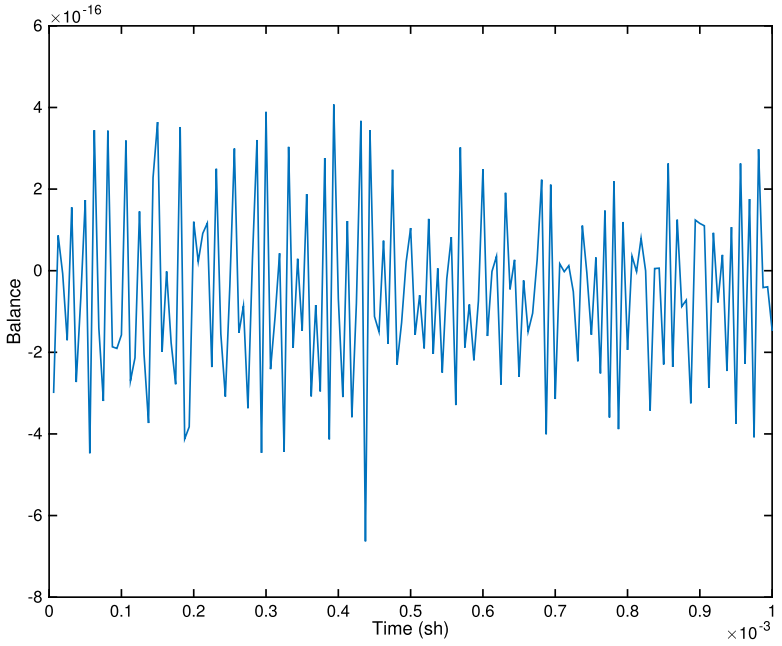

Fig. 9. Energy balance as a function of time for MMS problem.

Table 1
Initial condition values for $M_0 = 1.2$ shock problem.

Parameter	Pre-shock value	Post-shock value	Unit
ρ	1.00000000e+00	1.29731782e+00	g cm^{-3}
u	1.52172533e−01	1.17297805e−01	cm sh^{-1}
T	1.00000000e−01	1.19475741e−01	keV
e	1.44727998e−02	1.72914848e−02	Jk g^{-1}
$\mathcal{E}$	1.37201720e−06	2.79562228e−06	Jk cm^{-3}
$\mathcal{F}_0$	0.00000000e+00	0.00000000e+00	Jk cm^{-2} s^{-1}

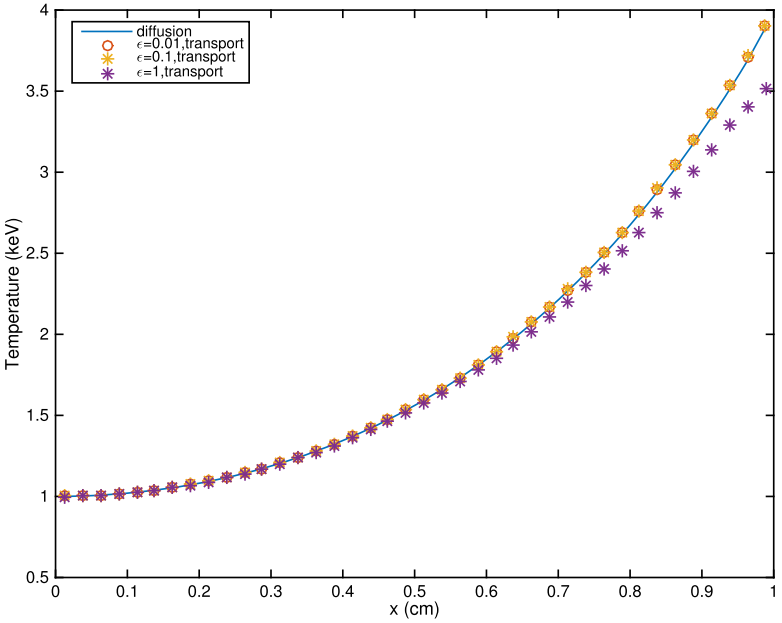

Fig. 10. The material temperature using different scale values.

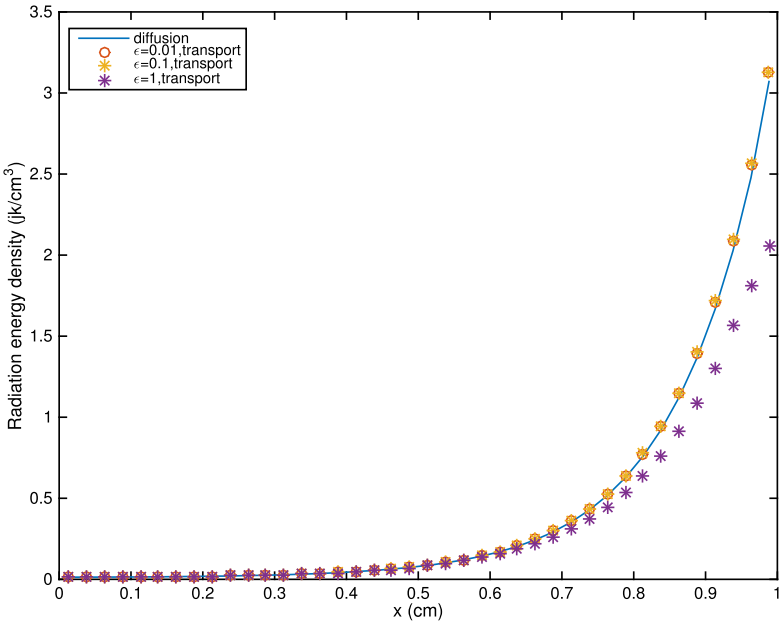

Fig. 11. The radiation energy density using different scale values.

Table 2
Initial condition values for $M_0 = 3$ shock problem.

Parameter	Pre-shock value	Post-shock value	Unit
ρ	1.00000000e+00	3.00185103e+00	g cm^{-3}
u	3.80431331e−01	1.26732249e−01	cm sh^{-1}
T	1.00000000e−01	3.66260705e−01	keV
e	8.68367987e−02	1.83229115e−02	Jk g^{-1}
$\mathcal{E}$	1.37201720e−06	2.46899872e−06	Jk cm^{-3}
$\mathcal{F}_0$	0.00000000e+00	0.00000000e+00	Jk cm^{-2} s^{-1}

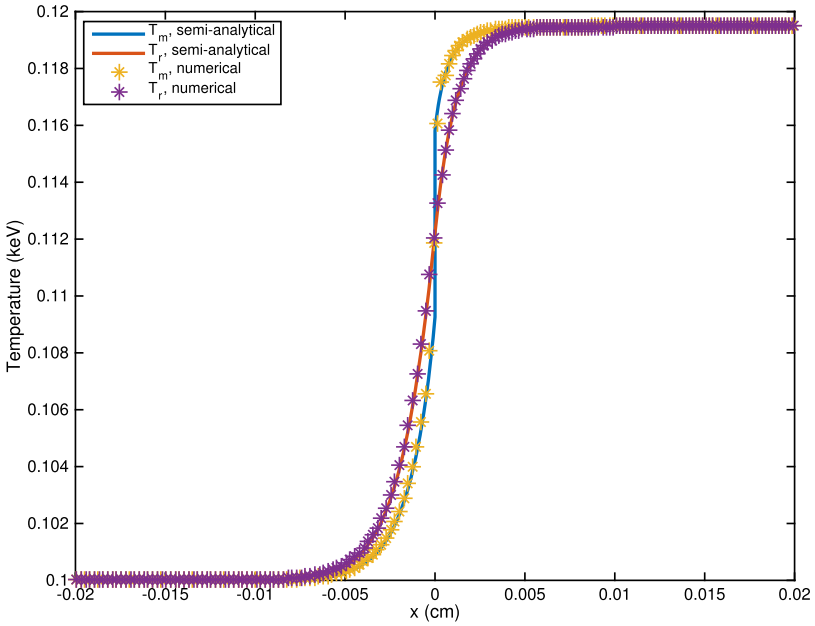

Fig. 12. $M_0 = 1.2$ radiative shock fluid and radiation temperature.

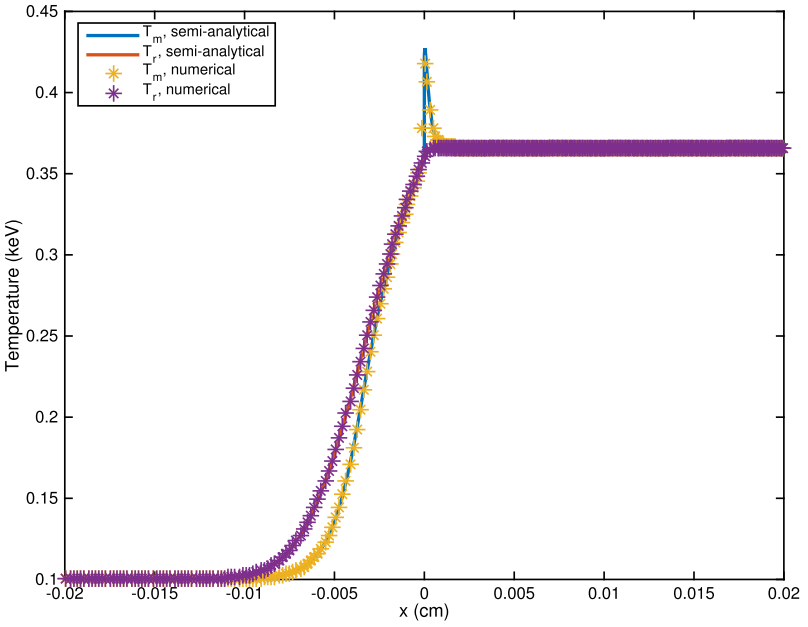

Fig. 13. $M_0 = 3$ radiative shock fluid and radiation temperature.

The parameters for both shock calculations were chosen as follows: $N_x = 4000$ spatial cells for $M_0 = 1.2$, $N_x = 5000$ spatial cells for $M_0 = 3$, a CFL condition of 0.5, and $\Delta t = 5 \times 10^{-5}$. The initial spatial domain was chosen as $[-0.25, 0.25]$ cm. The calculation was terminated when steady state was reached. The radiative fluid temperature T_m and radiation temperature $T_r = (\mathcal{E}/a)^{0.25}$ for $M_0 = 1.2$ are plotted in Fig. 12. Our numerical solutions agree well with the semi-analytical solutions.

The radiative fluid temperature T_m and radiation temperature T_r for $M_0 = 3$ are plotted in Fig. 13. Note that there is a Zel'dovich spike [18] with increased fluid temperature at the front of the shock. Our numerical solutions agree well with the semi-analytical solutions.

10. Conclusions

We have derived a HOLO VEF method for coupling high-order grey 1-D slab-geometry S_n radiation transport equations having a LLDG discretization with a low-order set of radiation moment and hydrodynamics equations having a MFEM discretization. The MMS method was employed for generating a benchmark solution and the results show that the HOLO VEF method is second order accurate in time and space. Another MMS solution was used to demonstrate that our HOLO VEF method preserves the thick diffusion limit. Moreover, our VEF method was tested on two shock problems, and the numerical solutions show excellent agreement with the semi-analytical solutions. In a previous paper [4], it was shown that the pure radiative transfer scheme (the S_n equations coupled to the radiation moment equations and a material temperature equation rather than the hydrodynamics equations) is well-behaved with unresolved spatial boundary layers in the equilibrium-diffusion limit, and yields accurate Marshak wave speeds even with strongly temperature-dependent opacities and relatively coarse meshes. These same properties carry over to our radiation-hydrodynamics scheme.

Overall we conclude, that our HOLO VEF approach yields a second-order accurate and efficient radiation-hydrodynamics scheme even though a LLDG spatial discretization is used for the high-order S_n equations, and a MFEM discretization is used for the low-order radiation-hydrodynamics equations.

In this work, we choose to nonlinearly converge the low-order radiation-hydrodynamics solutions within each VEF iteration. One could almost certainly improve efficiency by iterating on the low-order nonlinearities and the variable Eddington factors at the same time. However, optimization of such a iteration scheme will be strongly problem-dependent. Furthermore, the cost of an S_n sweep will dramatically increase in multidimensions, strongly impacting the optimization. Thus we suggest that a study of this iteration approach be carried out in the future.

CRediT authorship contribution statement

Jijie Lou: Formal analysis, Investigation, Software, Validation, Visualization, Writing – original draft. **Jim E. Morel:** Conceptualization, Funding acquisition, Methodology, Project administration, Resources, Supervision, Writing – review & editing.

Declaration of competing interest

The authors declare that they have no known competing financial interests or personal relationships that could have appeared to influence the work reported in this paper.

Acknowledgement

This work was performed under the auspices of the U.S. Department of Energy by Lawrence Livermore National Laboratory under Contract DE-AC52-07NA27344.

References

[1] M.L. Adams, E. Larsen, Fast iterative methods for discrete-ordinates particle transport calculations, Prog. Nucl. Energy 40 (1) (2002) 3–159.
[2] J.D. Edwards, J.E. Morel, D.A. Knoll, Nonlinear variants of the TR/BDF2 method for thermal radiative diffusion, J. Comput. Phys. 230 (2011) 1198–1214.
[3] V. Dobrev, T. Kolev, R. Rieben, High-order curvilinear finite element methods for Lagrangian hydrodynamics, SIAM J. Sci. Comput. 34 (2012) B606–B641.
[4] J. Lou, J.E. Morel, N. Gentile, A variable Eddington factor method for the 1-D grey radiative transfer equations with discontinuous Galerkin and mixed finite-element spatial differencing, J. Comput. Phys. 393 (2019) 258–277.
[5] R. Lowrie, J. Morel, J. Hittenger, The coupling of radiation and hydrodynamics, Astrophys. J. 521 (1999) 432–450.
[6] S.S. Olivier, J.E. Morel, Variable Eddington factor method for the sn equations with lumped discontinuous Galerkin spatial discretization coupled to a drift-diffusion acceleration equation with mixed finite-element discretization, J. Comput. Theor. Transp. 46 (6–7) (2018) 480–496.
[7] V.Y. Gol'din, A quasi-diffusion method of solving the kinetic equation, USSR Comput. Math. Math. Phys. 4 (1964) 136–149.
[8] E. Lewis, W.F. Miller, Computational Methods of Neutron Transport, American Nuclear Society, 1993.
[9] Ben C. Yee, S.S. Olivier, T.S. Haut, M. Holec, V.Z. Tomov, P.G. Maginot, A quadratic programming flux correction method for high-order dg discretizations, J. Comput. Phys. 419 (2020) 109696.
[10] C. Buet, B. Després, Asymptotic preserving and positive schemes for radiation hydrodynamics, J. Comput. Phys. 215 (2006) 717–740.
[11] C. Buet, S. Cordier, An asymptotic preserving scheme for hydrodynamics radiative transfer models, Numer. Math. 108 (2007) 199–221.
[12] J.F. Blachère, R. Turpault, An admissibility and asymptotic-preserving scheme for systems of conservation laws with source term on 2d unstructured meshes, J. Comput. Phys. 315 (2016) 98–213.
[13] E.W. Larsen, J. Morel, J. Warren, F. Miller, Asymptotic solutions of numerical transport problems in optically thick, diffusive regimes, J. Comput. Phys. 69 (1987) 283–324.
[14] S. Bolding, J. Hansel, J.D. Edwards, J.E. Morel, R.B. Lowrie, Second-order discretization in space and time for radiation-hydrodynamics, J. Comput. Phys. 338 (2017) 511–526.
[15] J. Warsa Densmore, A.K. Prinja, J. Morel, Manufactured solutions in the thick diffusion limit, Nucl. Sci. Eng. 166 (2010) 36–47.
[16] J. Morel, T. Wareing, K. Smith, A linear-discontinuous spatial differencing scheme for sn radiative transfer calculation, J. Comput. Phys. 128 (1996) 445–462.
[17] J. Ferguson, J. Morel, R. Lowrie, The equilibrium-diffusion limit for radiation hydrodynamics, J. Quant. Spectrosc. Radiat. Transf. 202 (2017) 176–186.
[18] R. Lowrie, J.D. Edward, Radiative shock solutions with grey nonequilibrium diffusion, Shock Waves 18 (2008) 129–143.